Supporting Information for

Ventral hippocampus interacts with prelimbic cortex during inhibition of threat response via learned safety in both mice and humans

Heidi C. Meyer[a,1], **Paola Odriozola**[b,1], **Emily M. Cohodes**[b], **Jeffrey D. Mandell**[c], **Anfei Li**[a], **Ruirong Yang**[a], **Baila S. Hall**[d], **Jason T. Haberman**[b], **Sadie J. Zacharek**[b], **Conor Liston**[e,f], **Francis S. Lee**[a,e,2,3], **Dylan G. Gee**[b,2,3]

[a]Department of Psychiatry, Weill Cornell Medicine, New York, NY 10065
[b]Department of Psychology, Yale University, New Haven, CT 06511
[c]Program in Computational Biology and Bioinformatics, Yale University, New Haven, CT 06511
[d]Department of Psychology, Brain Research Institute, University of California Los Angeles, Los Angeles, CA 90095
[e]Sackler Institute for Developmental Psychobiology, Weill Cornell Medicine, New York, NY 10065
[f]Feil Family Brain & Mind Research Institute, Weill Cornell Medicine, New York, NY 10065

[1]H.C.M. and P.O. were co-first authors and contributed equally to this work
[2]F.S.L. and D.G.G. were co-senior authors and contributed equally to this work
[3]To whom correspondence may be addressed. Email: fslee@med.cornell.edu or dylan.gee@yale.edu.

This PDF file includes:

Supplementary Text

Methods

Mice

Male mice (C57BL/6J) were purchased from The Jackson Laboratory (Bar Harbor, ME, USA). Mice were obtained at 8 weeks of age and allowed at least one week to acclimate to the colony room prior to surgery and behavioral training. Mice were maintained with a 12-hour light/dark cycle at 18°C - 22°C and had ad libitum access to water and food (LabDiet, PicoLab Rodent Diet 20). Mice were group housed in cages of 3-5 and randomly allocated to experimental groups. All mice were healthy with no obvious behavioral phenotypes, and none of the experimental mice were immune compromised. Experiments were carried out in accordance with the National Institutes of Health's Guide for the Care and Use of Laboratory Animals, and protocols were approved by the Weill Medical College of Cornell University's Institutional Animal Care and Use Committee.

Surgical Procedures

Mice were anesthetized approximately five minutes prior to the start of the operative procedures with a ketamine and xylazine cocktail (100mg/ml and 10mg/ml, respectively) at a dosage of 0.1mL per 10g of total body weight. Mice also received a preemptive analgesic injection of meloxicam (2mg/kg, subcutaneous). Each mouse was placed in a Kopf stereotaxic head frame equipped with blunted ear bars and a mouse incisor bar. The local anesthetic Bupivacaine (0.25%) solution was administered along the incision line between skull and head skin, followed by surgical exposure of the skull.

Holes were drilled in the skull unilaterally over virus infusion and fiber implantation sites using an electric drill mounted on a manipulator (David Kopf Instruments). All infusions were made with a 10µl Nanofil syringe (World Precision Instruments) equipped with a 33-gauge blunt needle and connected to an infusion pump (UMP, Micro4; World Precision Instruments). Target coordinates were defined by the Paxinos and Franklin's (4th Edition) mouse brain atlas (1). The coordinates to target the ventral hippocampus were: 3.2mm posterior and 3.1mm lateral to bregma at a depth of 3.2mm from brain surface. The coordinates to target PL were: 2.2mm anterior and 0.3mm lateral to bregma at a depth of 1.35mm from brain surface. The coordinates to target IL were: 1.65mm anterior and 0.3mm lateral to bregma at a depth of 2.2mm from brain surface. The coordinates to target BLA were: 1.5mm posterior and 3.0mm lateral to bregma at a depth of 3.65mm from brain surface. To serve as a cumulative measure of ventral hippocampal activity, one group of mice received infusions of the genetically modified calcium indicator GCaMP under a synapsin-promoter driven adeno-associated viral vector (AAV1-Syn-GCaMP6s-WPRE-SV40, viral titer = 2.5x10^13 GC/ml, Addgene Plasmid Repository). To isolate target-defined subpopulations of ventral hippocampal neurons, a Cre-recombinase activated strain of the GCaMP virus (AAV5-Syn-FLEX-GCaMP6s-WPRE-SV40, viral titer = 1.1x10^13 GC/ml, Addgene Plasmid Repository) was used to transduce neurons in the ventral hippocampus with the GCaMP molecule, while a second construct, rAAV2-retro/CAG-Cre (viral titer = 5.3x10^12 VP/ml, The Vector Core at the University of North Carolina at Chapel Hill) was used to isolate GCaMP expression to subpopulations of interest. The retro-Cre virus was infused into either PL, IL, or BLA. At each site GCaMP (200nl) or retro-Cre (150nl) viral constructs were infused at a rate of 50nl/min. The needle was left in place for 1 min before and 6 min after each infusion, then raised in depth by 0.1 mm and left for an additional minute before withdrawal from the brain. A mono fiber-optic cannula (Doric Lenses) with a 0.48 refractive index and a 400nm diameter was implanted into the ventral hippocampus immediately following injection of the virus(es), just above the viral injection site (~0.05mm above each depth indicated above). The implant was fixed to the skull using Metabond Quick Adhesive Cement

(Parkell Inc.). Recovery and expression of the transgenes was allowed to take place over the course of 4 weeks before the beginning of behavioral training.

Animal Behavior

Behavioral apparatus. Behavioral procedures were carried out in standard conditioning chambers (Med Associates). The chambers (30 × 24 × 27 cm) consisted of clear acrylic front and back walls, aluminum sides, stainless steel grid floors, and a clear acrylic top modified to include a centralized hole (5cm diameter) and access slot (9 x 0.6 cm) allowing an access point for the fiber photometry patch cord. Each chamber was outfitted with two speakers located 13cm above the grid floor, used to present the auditory conditioned stimuli, a 2.9kHz tone, or a 12.5kHz tone, both 80dB, played for 20s and counterbalanced as threat or safety. Delivery of a 1s 0.5mA footshock served as the aversive unconditioned stimulus (US). The two contexts were differentiated using a white acrylic cylindrical contextual insert and a white acrylic floor cover (Context B). Each chamber contained an LED Stimulus Light (50 lux; mounted 18cm above the grid floor; Context A) and a light box (125 lux; ceiling-mounted 52cm above the grid floor; Context B) to provide background illumination. In addition, differing olfactory cues were present between the contexts: Context A was scented with peppermint (1/1000 in ethanol) while Context B was scented with (-)-Limonene, 92% (1/1000 in ethanol). Each chamber was enclosed in a sound-attenuating cubicle (71 × 59 × 56 cm) with a 28V DC exhaust fan to provide airflow and background noise. The cubicles also contained surveillance cameras used to monitor the mice during behavioral training.

Behavioral procedures. For four consecutive days, all mice were trained to discriminate between threat and safety cues. Each day mice were acclimated to the conditioning chamber (Context A) for 2 minutes prior to any stimulus exposures. Mice were then exposed to intermixed presentations of threat and safety cues on a variable intertrial interval (ITI; 30-90 seconds) schedule. Presentations of the threat cue co-terminated with a mild footshock (0.5mA, 1s duration). Mice were exposed to 2 presentations of the threat cue and 30 presentations of the safety cue each day, with the trial order varied daily. Mice remained in the conditioning chamber for 1 minute after the final stimulus presentation before being returned to their home cages.

On day 5, the testing phase, mice were connected to a patch cord allowing for live recording of calcium signaling. Behavioral testing and fiber photometry recording took place in a novel conditioning chamber (Context B) in order to isolate cue-elicited behavioral responding from residual contextual fear. Following a 2-minute acclimation period to the testing chamber separate groups of mice were exposed to 10 presentations of a threat, safety, or compound cue in the absence of shock. Tone presentations lasted for 20s with an ITI of 60s. After the final tone presentation, mice remained in the chamber for 1 minute before being disconnected from the patch cord and returned to their home cages.

Behavioral analysis. Video Freeze® software (Med Associates) was used to control experiments, and all trials were videotaped for manual analysis. Freezing was defined as the absence of visible movement except that required for respiration (2). The percentage time spent freezing was calculated by dividing the amount of time spent freezing during the tone by the total duration of the tone. Freezing behavior was then averaged across the 10 trials for each condition (threat, compound, safety) and subjected to a one-way ANOVA followed by a linear contrast for between-group analysis. Each hypothesis was tested at a level of significance $\alpha = 0.05$.

Fiber Photometry

Four weeks following recovery from surgery, mice underwent conditioned inhibition training (i.e., acquisition phase; Days 1-4; Fig. 1), and GCaMP signal was recorded during the testing phase (Day 5; Fig. 1). The fiber photometry rig was based on a design described in detail elsewhere (3, 4). A 470 nm LED (Thorlabs) modulated at a frequency of 521 Hz and passed through a filter (Semrock, FF02-472/30) and coupled to a 0.48 NA, 400 µm core optical fiber patch cord (Doric). Light from the LED served to excite neurons such that those neurons expressing the GCaMP emitted an activity-dependent fluorescent signal (4, 5). The fluorescent signal was also collected by the fiber-optic implant, separated from the excitation light using a dichroic (Semrock, FF495-Di03), passed through a single band filter (Semrock, FF01-535/50), focused on a photodetector (Newport, Model 2151), and recorded by a real-time processor (Tucker Davis Technologies). A pulse from the behavioral system (Video Freeze® software) was also passed to the processor allowing fluorescent signal to be time-locked to stimulus presentations.

Analysis of Fiber Photometry Data

Fiber photometry data were analyzed in MATLAB (MathWorks) where the fluorescent signal from each mouse was normalized to account for photobleaching across the session by calculating the ΔF/F. To do this, the median value of an 80s window (40s before and 40s after a given data point) was calculated. This value was then subtracted from each data point across the 15.5-minute recording period, and each outcome was divided by the same median. The data from each mouse were transformed to a z-score to allow comparison of calcium signal magnitude between mice. The data from each trial were individually normalized by subtracting the mean z-score across the 10s preceding a given trial from each data point across the trial. To analyze neural activity between conditions, the mean z-score was obtained by averaging across the 10 trials for each condition (threat, compound, safety). Means were compared using a one-way ANOVA followed by a linear contrast for between-group analysis. A linear regression analysis was used to investigate the relationship between mean z-score and average freezing behavior. For analysis of the temporal distribution of peak calcium signal, the highest 5% of z-score values was isolated for each trial and the corresponding time of occurrence during the trial was recorded. The proportion of data points occurring within sequential 5s bins of each trial (time epochs of 0-5s, 6-10s, 11-15s, and 16-20s) was calculated and subjected to a two-way repeated-measures ANOVA. A Tukey HSD test with the first time epoch (0-5s) as the comparison cell was used as a follow-up to significant interactions. Reported p values following Tukey HSD tests are multiplicity adjusted. The mean magnitude of peak calcium signal was obtained by averaging across the 10 trials for each condition, and means were compared using a one-way ANOVA followed by a linear contrast for between-group analysis. Each hypothesis was tested at a level of significance $\alpha = 0.05$.

Histology

After the completion of behavioral testing and fiber photometry recordings, mice were anesthetized with an overdose of sodium pentobarbital and transcardially perfused with 30 mL of 0.9% saline, followed by 120 mL of 4% paraformaldehyde in 0.01 M sodium phosphate buffer (pH 7.4), at a flowing rate of 25 mL per min using a Perfusion Two Automated Pressure Perfusion system (Leica Microsystems, Buffalo Grove, IL, USA). The brains were then removed and post-fixed with 4% paraformaldehyde in 0.01 M sodium phosphate buffer (PB) at 4°C overnight and transferred to a sucrose solution (30% sucrose in 0.1 M PB) at 4°C for 48 hours. Coronal sections (40µm) were prepared using a freezing microtome. The sections were mounted on chromium/gelatin-coated slides and cover-slipped by water-soluble glycerol-based mounting medium containing 4,6-diamidino-2-phenylindole (DAPI) and sealed with nail polish.

Sections were analyzed to verify expression of the GCaMP and placement of the optical fiber using Stereo Investigator software (MicroBrightField Bioscience) and a fluorescent microscope (Nikon eclipse). Mice with inaccurate targeting were eliminated from the study.

Humans

Participants were recruited through flyers and online postings in the New Haven area. Individuals with contraindications for MRI scanning (e.g., metal implants, pacemakers, metal foreign bodies, braces, claustrophobia, reported possibility of pregnancy for female participants), chronic medical illness, and neurological disorders were excluded.

For functional MRI (fMRI) analyses, subjects were excluded if their in-scanner mean absolute translational or rotational motion in any of the 6 rigid directions was greater than 2 mm or 2°, respectively, if their mean relative (timepoint to timepoint) motion was greater than 0.2 mm, or if the percentage of data that would need to be regressed out due to motion outlier timepoints exceeded 15% (ref. 6; see details in fMRI Individual-level Analyses section). This resulted in the removal of data from three participants from all fMRI analyses. One additional participant was excluded due to technical errors in the data processing pipeline, for a sample of 50 participants for fMRI analyses. In this sample, motion was assessed using mean framewise displacement (FD; Table S1), which is a summary measure of the 6 rigid parameters, and was calculated as described in (6).

Study procedures

Each participant completed two separate visits to the laboratory. At the first visit, participants completed a general assessment of IQ (Wechsler Abbreviated Scale of Intelligence; WASI; ref. 7), handedness (Edinburgh Handedness Questionnaire; ref. 8), and a clinical interview (Anxiety Disorders Interview Schedule for DSM-5; ref. 9) to assess eligibility. Eligible participants were invited to participate in the MRI scan at the second visit.

Task design.

The experiment consisted of four phases: acquisition, testing, extinction, and reversal. During the acquisition phase, participants viewed 20 trials of the threat cue (CS+), which was reinforced with the US on 50% of trials (i.e., 10 reinforced and 10 non-reinforced threat cue trials), and 10 trials of the safety cue, which was never paired with the US. The acquisition phase was presented in a blocked format (i.e., all threat cues were presented sequentially and all safety cues were presented sequentially). During the testing phase, the same threat (50% reinforcement with the US) and safety cues were presented, and the threat and safety cues were also paired together (i.e., shown simultaneously in a compound cue) to test for transfer of the safety cue to reduce fear to the threat cue ("summation test"; ref. 10). The threat cue and a novel stimulus were also paired together as a control condition to rule out the reduction of fear via novelty (i.e., external inhibition); this novel compound condition was not analyzed in the present study given that this condition was not included in the parallel task with mice. The testing phase was divided into two consecutive runs (~ 7 minutes each) to reduce the chance of excessive motion associated with a longer fMRI scan. In total, the testing phase included 12 trials of each condition (6 trials in each of the two runs), and the order of trials was fully randomized. During the extinction phase, participants were presented with the previously-learned threat cue without the US (10 trials) and the safety cue (10 trials) in a randomized order. During the reversal phase, the previously-learned safety cue was reinforced with the US on 50% of trials to test for slowing of fear acquisition ("retardation test"; ref. 10). The reversal phase included 10 trials of the now-extinguished original threat cue (which was switched to the “safety” condition during reversal) and 20 trials of the original safety cue (which was switched to the “threat” condition during reversal); (i.e., 10 reinforced trials, 10 non-reinforced trials) in separate blocks to parallel the acquisition phase. In all task phases except extinction, partial

reinforcement (50%) was used in order to enable assessment of the physiological and BOLD responses to the learned CS alone, without a potentially confounding influence of the response to the US (10). Thus, only non-reinforced threat trials were included in our analyses.

In an event-related design, each stimulus was presented for 1500ms, at which point a white dot appeared in the center of the shape (presented for 500ms; Fig. 1B, Sample trial). For reinforced trials of the threat cue (CS+), the US onset at the same time as the dot in the center of the shape, lasted 500ms, and co-terminated with the threat cue. To maintain engagement, participants were instructed to make a button press when the dot appeared in the center of the shape on each trial. Participants were told that their button press would not do anything and that it was simply to ensure that they were paying attention. A fixed ITI of 10 seconds separated each trial in order to allow for stabilization of the blood-oxygen level dependent (BOLD) and skin conductance response (SCR) signals (Fig. 1B, Sample trial). The assignment of the three shapes to the three stimulus types (threat, safety, or novel cue) was counterbalanced across participants.

Two modifications to the task design were implemented during data collection to further optimize the conditioned inhibition task. Out of the 50 subjects in the present study, 21 completed version A of the task; the remaining 29 subjects completed version B. First, in version A, during the acquisition phase, the order of blocks (i.e., block of threat cues, block of safety cues) was counterbalanced across subjects, such that a total of 13 eligible participants completed the safety block first and 8 completed the threat block first. In version B, all participants completed the threat block first to increase alertness and engagement during the acquisition phase. Second, in version A, during the threat block in the acquisition phase, the reinforced and non-reinforced trials were randomized and fixed, with the same order of stimuli across these 21 participants. In version B, the reinforced and non-reinforced threat cue trials were pseudo-randomized within the threat block with a unique presentation order for each participant. The pseudo-randomization included the constraint that no more than 3 consecutive repetitions of the same cue were permitted in order to ensure a lack of predictable order and prevent an early onset of the extinction process (10).

We note here that the MRI data for all subjects who completed version A of the task were collected using Siemens software version VE11B on one Siemens Magnetom Prisma scanner and data for all subjects who completed version B were collected on a different Siemens Magnetom Prisma scanner with software version VE11C at the same imaging center. A single between-subjects variable (dummy-coded) was used as a covariate in all analyses to control for the task version completed (A vs. B) and scanner/software (VE11B vs. VE11C), as these changes were completely correlated.

MRI acquisition parameters.

Of the 50 subjects included in fMRI analyses, 21 participants were scanned on one Siemens Magnetom Prisma scanner (software version VE11B) and 29 subjects were scanned on a different Siemens Magnetom Prisma scanner (software version VE11C) at the same imaging center. Scan parameters were based on nationwide neuroimaging data collection for the Adolescent Brain Cognitive Development (ABCD) Study (11). Sequences were updated and optimized for the Siemens Prisma software upgrade to VE11C, consistent with the ABCD Study. A whole-brain high-resolution T1-weighted anatomical scan magnetization-prepared rapid acquisition gradient echo (MPRAGE; 1070 ms TI, 2500 ms TR; 2.9 ms TE; 8° flip angle; 256 mm field of view (FoV); 176 slices in sagittal plane; 256 x 256 matrix; 2x parallel imaging; 1.0 x 1.0 x 1.0 mm resolution) was acquired for each subject for transformation, co-registration, and localization of functional data into Montreal Neurological Institute (MNI) space. A whole-brain high-resolution T2-weighted fast spin echo was also acquired for detection and quantification of white matter lesions and cerebral spinal fluid (3200 ms TR; 565 ms TE; variable flip angle;

256 mm FoV; 176 slices in sagittal plane; 256 x 256 matrix; 2x parallel imaging; 1.0 x 1.0 x 1.0 mm resolution).

During the conditioned inhibition task, high spatial and temporal resolution multiband echo planar imaging (EPI) fMRI scans were collected with fast integrated distortion correction across a total of five runs. Sixty axial slices (7 mm thickness) covering the whole brain were imaged using a T2*-weighted EPI sequence (800 ms TR; 30 ms TE; 52° flip angle; 216 FoV; 90 x 90 matrix; 2.4 x 2.4 x 2.4 mm resolution; 6 multiband acceleration factor with interleaved acquisition). To enable accurate spatial distortion correction, a pair of spin echo EPI scans with opposite phase encoding directions was collected prior to each block of functional scans, in accordance with Human Connectome Project (HCP) guidelines (12).

Analysis of fMRI Data

fMRI preprocessing. Participant-level volume-based images were used in the analyses outlined below. The preprocessing of these task-based functional data involved gradient distortion correction, EPI field map preprocessing and distortion correction, motion correction, nonlinear registration to the MNI template (MNI 152, 2 mm space), and grand-mean intensity normalization. Specifically, the EPI fMRI images were corrected using spin echo "fieldmap" EPI scans with opposite phase encoding directions, resulting in opposite spatial distortion. As implemented in the HCP minimal preprocessing pipeline, the two fieldmap images were aligned using a nonlinear optimization to estimate the distortion field and enable the removal of spatial and intensity distortions from the fMRI images (13–16). Volumetric data (i.e., results from the fMRIVolume preprocessing step in the HCP Minimal Preprocessing Pipeline) were used for further analyses.

fMRI individual-level analyses. In the lower-level FEAT analysis, predictors for each task condition (including separate predictors for the anticipation and response periods for each condition; Fig. 1B, Sample trial) were convolved with a double-gamma canonical hemodynamic response function (HRF). Temporal derivatives of each predictor were added as a confound term to the GLM to account for slice-timing differences and variability in the HRF delay across regions. Timeseries were high-pass filtered with a cutoff of 90 s (estimated for our specific task design using FSL's *cutoffcalc* function) and prewhitened within FILM to correct for autocorrelations in the timeseries.

Rigorous motion correction was implemented to limit the potential effects of motion on task-related results. Standard and extended motion parameters output from FSL's MCFLIRT (17) during HCP minimal preprocessing were added as nuisance regressors in each participant's lower-level design matrices. Additionally, FSL's *fsl_motion_outliers* function was used to detect timepoints that were corrupted by large motion in each participant's data. Specifically, outliers were defined using FD as the motion metric (6) and the default definition of outliers (i.e., as in a boxplot: 1.5 times the interquartile range above the upper quartile; ref. 18). This function created a confound matrix with a regressor for every outlier timepoint detected that was added to the subject-specific lower-level design matrix to remove (i.e., regress out) the effect of these timepoints on the results. This approach is intended to address the effects of intermediate to large motion, which corrupt images beyond anything that the linear motion parameter regression methods can fix, while not disrupting the temporal structure of the timeseries (https://fsl.fmrib.ox.ac.uk/fsl/fslwiki/FSLMotionOutliers). Following this procedure, the sample had a total range of 0 - 92 timepoints (0 - 8.85% of data) regressed out of their individual lower-level analyses (summed across two testing runs), with a mean of 34.55 (3.32%) and standard deviation of 24.23 (2.33%) timepoints (Table S1).

Inclusion of covariates of no interest. In order to determine which covariates should be included in the models, full Pearson's correlation matrices were computed for variables of interest and the following variables of no interest: age (calculated in years with 3 decimal places), sex (dummy-coded), IQ, and task version/scanner (dummy-coded). No significant

correlations were found between hippocampal activation, hippocampal functional connectivity, or SCR measures with age or IQ. Therefore, these variables were not included in subsequent analyses. Significant or trend-level correlations were found between variables of interest with sex and task version/scanner, thus these covariates were included in all analyses.

Activation analysis. Extracted values for mean percent signal change in the ventral hippocampus for each condition were input to SPSS (www.ibm.com/analytics/spss-statistics-software) for further analysis. Separate repeated-measures analyses of covariance (ANCOVAs) were performed for region of interest (ROI) mean parameter estimates with a within-subjects factor of condition (threat, safety, safety compound).

Functional connectivity analysis. The same ventral hippocampus ROI as defined in the analyses of activation in the main text was used as the seed in a generalized psychophysiological interaction (gPPI) analysis to characterize task-based functional connectivity (19). The dACC ROI was defined using the probabilistic Harvard-Oxford atlas bilateral anterior cingulate and paracingulate regions, which were then divided into subregions by drawing a plane at the genu of the corpus callosum, as per (20). The anterior vmPFC ROI used in the present study was derived from (21), implemented in AFNI, converted to MNI space, and combined (i.e., right and left hemispheres) to form a bilateral ROI using the *fslmaths add* command. Lastly, the BLA ROI was derived from FSL's Juelich histological atlas: stereotaxic probabilistic maps of cytoarchitectonic boundaries generated by (22), and combined (i.e., right and left hemispheres) to form a bilateral ROI using the *fslmaths add* command.

In the lower-level FEAT analysis, predictors for each task condition were convolved with a double-gamma canonical HRF. The timeseries for the ventral hippocampus seeds (right and left, separately) were extracted using FSL's *meants* command and input as explanatory variables in each model. Interactions between the physiological variable (i.e., the ventral hippocampus seed timeseries) and each of the psychological variables (i.e., each task condition) were computed and included in the design matrix as the variables of interest. Temporal derivatives of each psychological predictor were added as a confound term to the GLM to account for slice-timing differences and variability in the HRF delay across regions. Motion correction and filtering were consistent with the analyses of activation reported above. Functional connectivity estimates for both the bilateral dACC and bilateral anterior vmPFC were extracted using FSL's featquery tool and input to SPSS for further analyses. Consistent with the ROI-based activation analyses, three participants were excluded from this analysis due to excessive motion in the scanner. Three additional participants were excluded from this analysis due to technical errors in the FSL processing pipeline, resulting in a subsample of n=48 for this analysis.

Analysis of Physiological data

Data were visually inspected for quality assurance, and subjects with SCR levels below 3 microsiemens (muS) on > 75% of trials were excluded from further SCR analysis. SCR data for the acquisition and testing phases of the task were analyzed using the GLM method in PsychoPhysiological Modeling (PsPM) software implemented in MATLAB (previously SCRalyze; www.pspm.sourceforge.net). Data were downsampled to 5 Hz and filtered with the default Butterworth bandpass filter, which is a unidirectional filter with cutoff frequencies of 0.05 and 5 Hz. A standard GLM was constructed in PsPM based on the evoked SCR with a response window of 0.5 to 6.5 seconds following stimulus presentation (23–25). Instead of using the canonical parameter estimates (i.e., beta coefficients) from the linear model, PsPM reconstructs the estimated evoked SCR and measures the peak amplitude over the response window which is used as an estimate of the amplitude of evoked sympathetic nerve activity (referred to as "recon" values in PsPM; ref. 25).

Following processing in PsPM, resulting reconstructed values for each condition (i.e., threat, safety, and safety compound) for each subject during the testing phase of the

conditioned inhibition task (Fig. 1B) were entered into a repeated-measures ANCOVA in SPSS. Twelve participants were excluded due to low overall SCR levels following visual quality assurance. Three additional subjects were excluded due to missing SCR or task event data. Finally, only participants who showed sustained learning, that is, those who showed a positive non-zero difference in mean SCR response to the threat cue versus the safety cue during the first half of the testing phase, were included. This resulted in a subsample of n=22 participants for the SCR analyses.

Secondary SCR analyses. To verify whether the quality assurance procedure was appropriate for inclusion of subjects in analyses of physiological data in the main text, an ANCOVA was conducted with a subsample of participants defined using a more stringent quality assurance threshold. Results were consistent with those in the main text, even when the sample was defined using a more stringent quality assurance measure in which all subjects' SCR signal was above .3 microsiemens throughout the entirety of the task (n=20), $F(2,36) = 3.82$, $p = .033$, $\eta_p^2 = .193$.

Though it is common to exclude non-learners from analyses of SCR (10), we also performed a secondary analysis of SCR data in which we did not exclude subjects based on a lack of sustained learning during the initial testing phase of the task (n=39). There was no significant effect of condition on SCR response in this model, $F(2,70) = 0.35$, $p = .709$, $\eta_p^2 = .010$.

Code availability

The custom written code files for fiber photometry data processing and human imaging analyses are available from the corresponding author upon reasonable request.

Data availability

Data used for these studies have been deposited in the Open Science Framework Repository (https://osf.io/nqryd/?view_only=dbcea56e594c41a1b741da18db70d6bd) and are available upon reasonable request to the corresponding author.

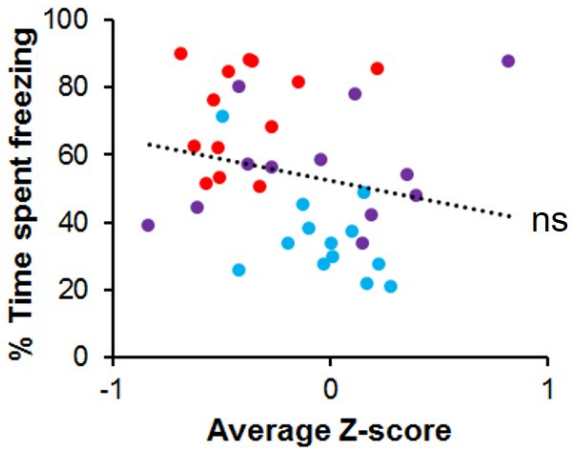

Fig. S1. Cumulative ventral hippocampal activity is not associated with freezing behavior. A linear regression revealed that mean z-score of calcium signal did not correlate with average freezing behavior, p = .189, η^2 = .05. Threat condition: n=13; Compound condition: n=12; Safety condition: n=13. ns = not significant.

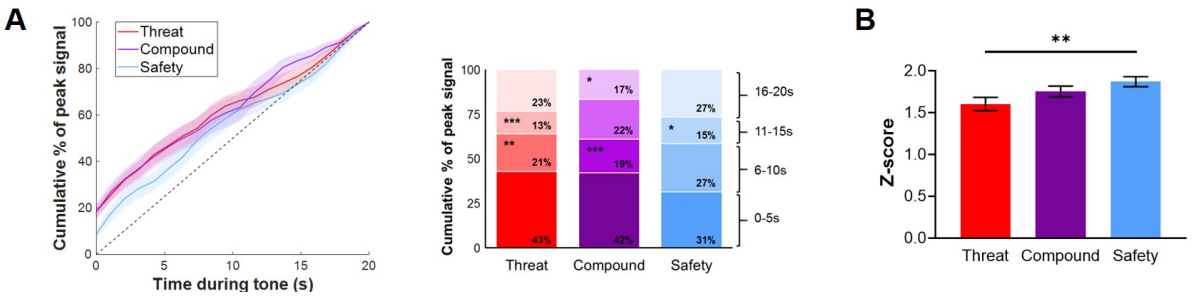

Fig. S2. Peak calcium signal in the cumulative ventral hippocampus differs by condition. A. Timeseries of peak calcium signal. (Left) Cumulative frequency distribution of proportion of peak calcium signal across the 20s cue by condition. Dashed line is included as a depiction of evenly distributed signal. (Right) Quantification of proportion of peak calcium signal by 5s epochs. The timeseries for peak calcium signal differed between threat, safety, and compound cues. The threat condition showed a significantly greater proportion of peak calcium signal during 0-5s than 6-10s (Tukey HSD, $p = .005$) and 11-15s (Tukey HSD, $p < .001$) . The compound condition showed a significantly greater proportion of peak calcium signal during 0-5s than 6-10s (Tukey HSD, $p < .001$) and 16-20s (Tukey HSD, $p = .051$). The safety condition showed a significantly greater proportion of peak calcium signal during 0-5s than 11-15s (Tukey HSD, $p = .023$). **B. Peak calcium signal magnitude.** Analysis of peak calcium signal magnitude shows ventral hippocampal activity differences during threat processing and conditioned inhibition. Mean magnitude of peak calcium signal showed a linear across threat, compound, and safety cues, $p = .009$, $\eta^2 = .18$. Threat condition: n=13; Compound condition: n=12; Safety condition: n=13. All error bars show +/- 1 SEM. *$p < .05$, **$p < .01$, ***$p < .001$.

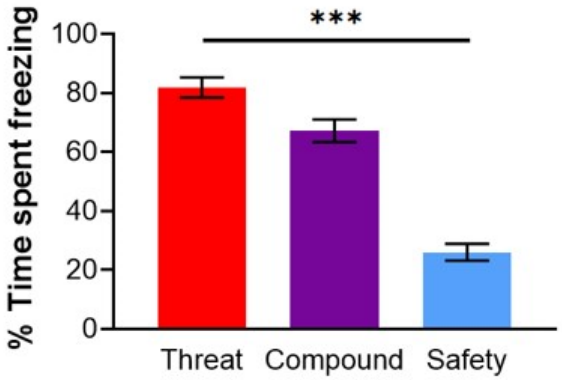

Fig S3. Task-related behavioral responses in mice expressing GCaMP-FLEX in prelimbic-targeted ventral hippocampal neurons. Mean percentage of time spent freezing by task condition in the testing phase revealed a linear effect in which freezing to threat cue was highest and to safety cue was lowest, $p < .001$, $\eta^2 = .75$. Threat condition: n=13; Compound condition: n=13; Safety condition: n=16. All error bars show +/- 1 SEM. ***$p < .001$.

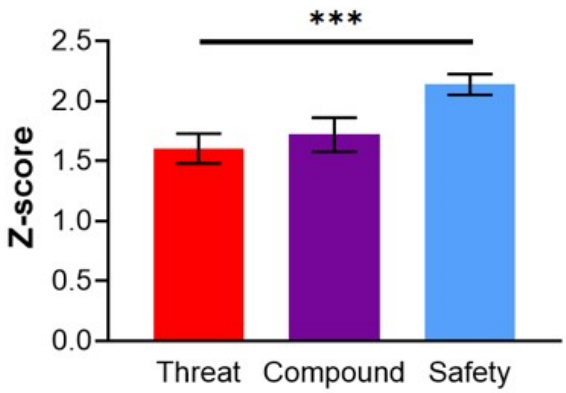

Fig. S4. Peak calcium signal magnitude in mice expressing GCaMP-FLEX in prelimbic-targeted ventral hippocampal neurons. Mean magnitude of peak calcium signal showed a linear increase across threat, compound, and safety cues, $p = .002$, $\eta^2 = .22$. Threat condition: n=13; Compound condition: n=13; Safety condition: n=16. All error bars show +/- 1 SEM. ***$p <$ .001.

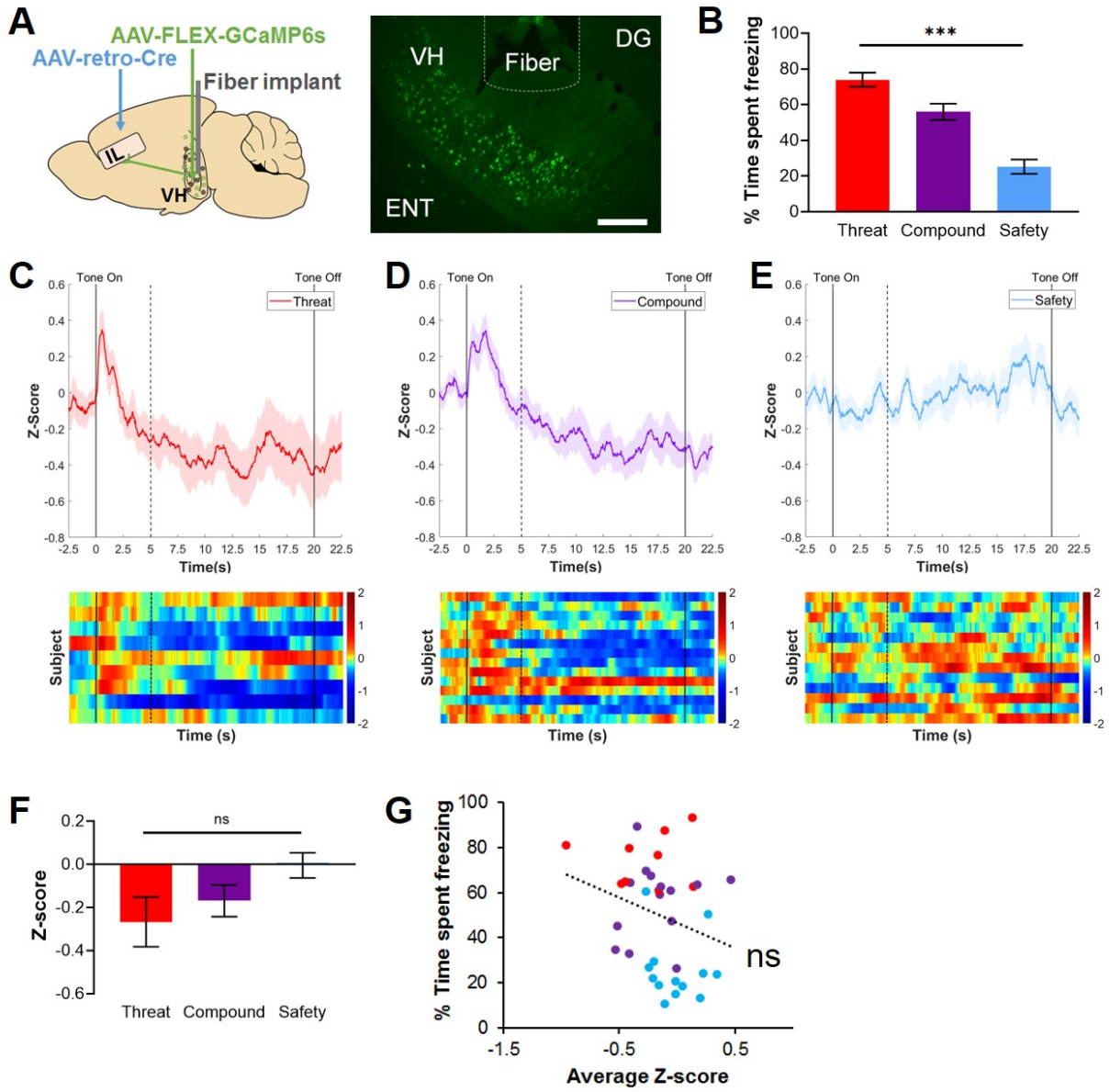

Fig. S5. Infralimbic-projecting ventral hippocampal neurons in mice. A. Schematic of fiber photometry targeted to infralimbic-projecting ventral hippocampal neurons in mice. (Left) Schematic of injection site for AAV-FLEX-GCaMP6s (ventral hippocampus), injection site for retro-Cre (infralimbic cortex) and fiber placement (ventral hippocampus). (Right) Representative example of GCaMP expression and fiber placement in ventral hippocampal cell bodies (10x magnification, bar = 200μm). DG = dentate gyrus; ENT = entorhinal cortex; IL = infralimbic cortex; VH = ventral hippocampus. **B. Task-related behavioral responses in mice.** Mean percentage of time spent freezing by task condition in the testing phase revealed a linear effect in which freezing to threat cue was highest and safety cue was lowest, $p < .001$, $\eta^2 = .63$. Threat condition: n=9; Compound condition: n=14; Safety condition: n=13. **C-E. Fiber photometry traces.** Trace of z-scored calcium signal and corresponding heatmaps for the threat condition **(B)**, compound condition **(C)** and safety condition **(D)**. Solid lines indicate tone onset (0s) and offset (20s). Dashed line indicates tone-onset induced activity for corresponding timeseries data. **F. Neural activity by condition in mice.** Mean z-score of calcium signal recorded from

infralimbic-projecting ventral hippocampal neurons showed no difference in neural activity between conditions, $p = .087$, $\eta^2 = .14$. Threat condition: n=9; Compound condition: n=14; Safety condition: n=13. **G. Relationship between neural activity and freezing behavior.** A linear regression revealed that mean z-score of calcium signal did not correlate with average freezing behavior, $p = .120$,$\eta^2 = .07$. All error bars show +/- 1 SEM. ***$p < .001$. ns = not significant.

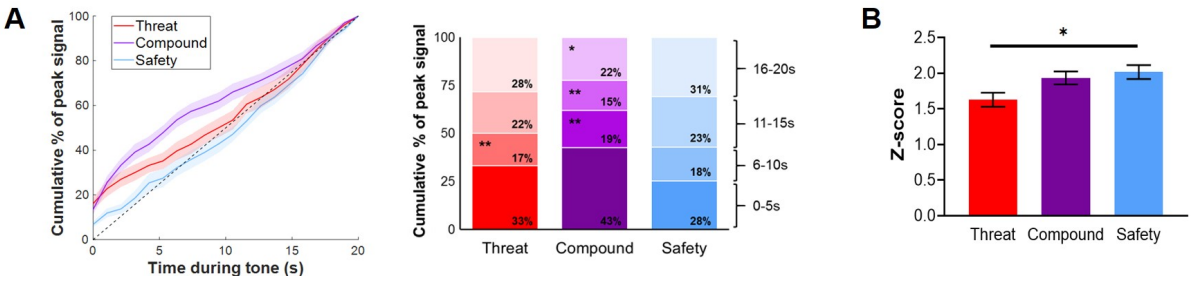

Fig. S6. Peak calcium signal in infralimbic-projecting ventral hippocampal neurons differs by condition. A. Timeseries of peak calcium signal. (Left) Cumulative frequency distribution of proportion of peak calcium signal across the 20s cue by condition. Dashed line is included as a depiction of evenly distributed signal. (Right) Quantification of proportion of peak calcium signal by 5s epochs. The timeseries for peak calcium signal differed between threat, safety, and compound cues. The threat condition showed a significantly greater proportion of peak calcium signal during 0-5s than 6-10s (Tukey HSD, p = .009). The compound condition showed a significantly greater proportion of peak calcium signal during 0-5s than 6-10s, 11-15s (Tukey HSD, ps < .001) and 16-20s (Tukey HSD, p = .016). **B. Peak calcium signal magnitude.** Mean magnitude of peak calcium signal showed a linear increase across threat, compound, and safety cues, p = .014, η^2 = .17. Threat condition: n=9; Compound condition: n=14; Safety condition: n=13. All error bars show +/- 1 SEM. *p < .05, **p < .01.

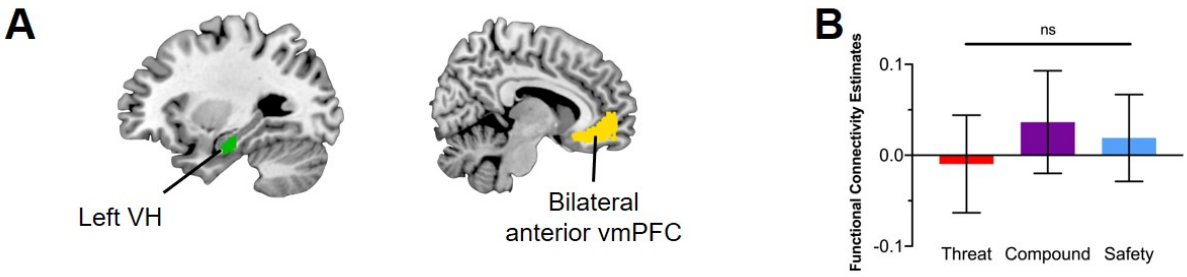

Fig. S7. Ventral hippocampus to anterior ventromedial prefrontal cortex functional connectivity in humans. A. Regions of interest. The left ventral/anterior hippocampus (VH) region of interest (ROI; green) examined in the present study was obtained from (19). The bilateral anterior ventromedial prefrontal cortex (anterior vmPFC) ROI (yellow) was obtained from (21). A generalized psychophysiological interaction (gPPI) was implemented in FSL to extract estimates of functional connectivity between these two regions. **B. Functional connectivity results.** No significant effect of condition on functional connectivity was observed, n=48, p = .782, η_p^2 = 0.006. All error bars show +/- 1 SEM. ns = not significant.

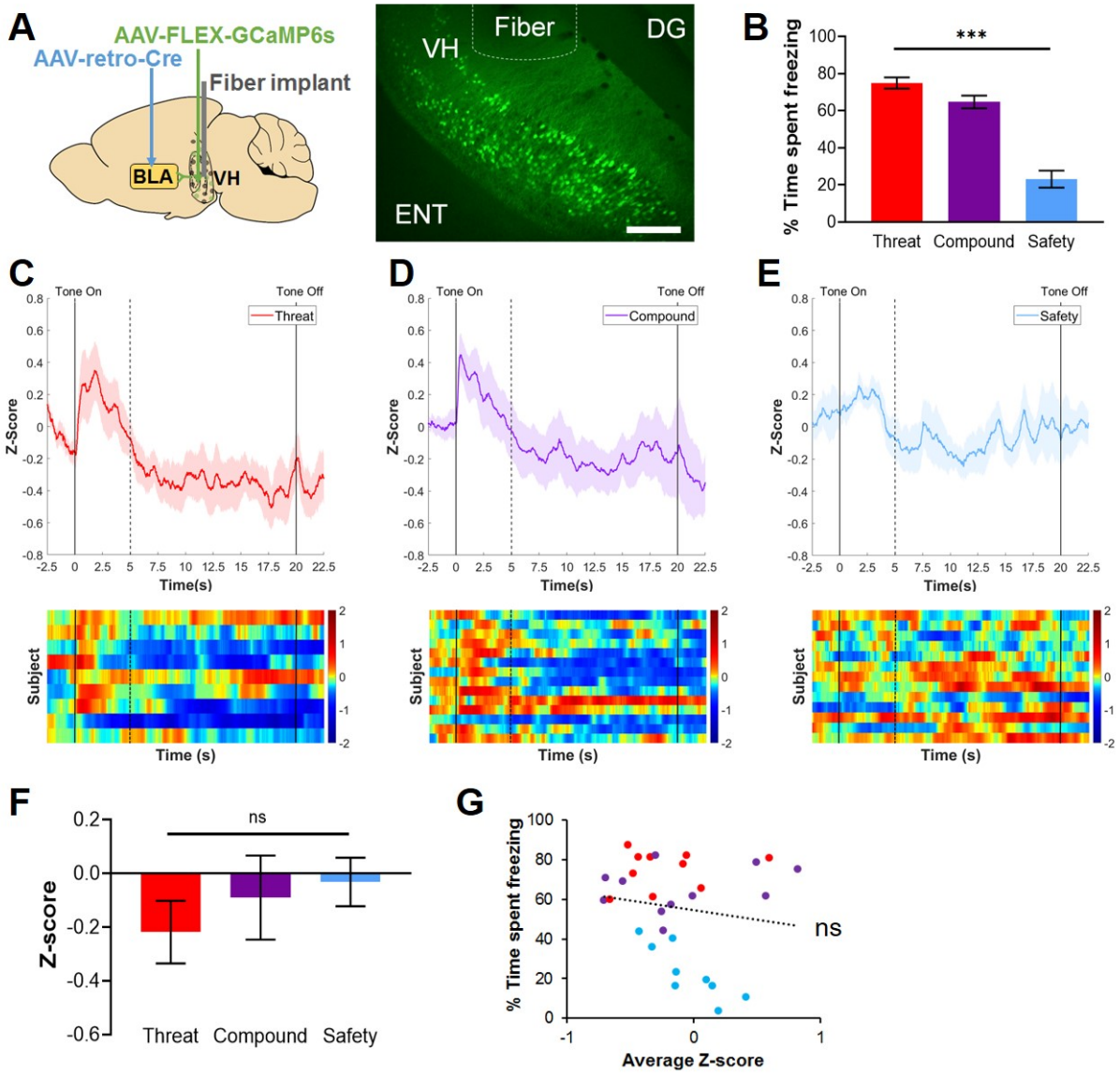

Fig. S8. Basolateral amygdala-projecting ventral hippocampal neurons in mice. A. Schematic of fiber photometry targeted to basolateral amygdala-projecting ventral hippocampal neurons in mice. (Left) Schematic of injection site for AAV-FLEX-GCaMP6s (ventral hippocampus), injection site for retro-Cre (basolateral amygdala) and fiber placement (ventral hippocampus). (Right) Representative example of GCaMP expression and fiber placement in ventral hippocampal cell bodies (10x magnification, bar = 200μm). BLA = basolateral amygdala; DG = dentate gyrus; ENT = entorhinal cortex; VH = ventral hippocampus. **B. Task-related behavioral responses in mice.** Mean percentage of time spent freezing by task condition in the testing phase revealed a linear effect in which freezing to threat cue was highest and to safety cue was lowest, $p < .001$, $\eta^2 = .70$. Threat condition: n=10; Compound condition: n=11; Safety condition: n=9. **C-E. Fiber photometry traces.** Trace of z-scored calcium signal and corresponding heatmaps for the threat condition **(B)**, compound condition **(C)**, and safety condition **(D)**. Solid lines indicate tone onset (0s) and offset (20s). Dashed line indicates tone-onset induced activity for corresponding timeseries data. **F. Neural activity by condition in mice.** Mean z-score of calcium signal recorded from basolateral amygdala-projecting ventral hippocampal neurons showed no difference in neural activity between

conditions, $p = .595$, $\eta^2 = .04$. **G. Relationship between neural activity and freezing behavior.** A linear regression revealed that mean z-score of calcium signal did not correlate with average freezing behavior, $p = .403$, $\eta^2 = .03$. All error bars show +/- 1 SEM. ***$p < .001$. ns = not significant.

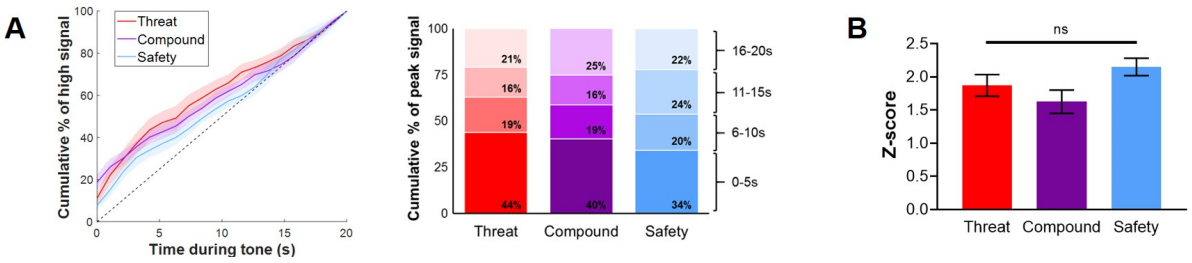

Fig. S9. Peak calcium signal in basolateral amygdala-projecting ventral hippocampal neurons does not differ by condition. A. Timeseries of peak calcium signal. (Left) Cumulative frequency distribution of proportion of peak calcium signal across the 20s cue by condition. Dashed line is included as a depiction of evenly distributed signal. (Right) Quantification of proportion of peak calcium signal by 5s epochs. While all three conditions exhibited a greater proportion of peak calcium signal occurring at tone onset, 0-5s, relative to all other epochs, $p < 0.001$, $\eta^2 = .38$, the timeseries of peak calcium signal did not differ between conditions, $p = .421$, $\eta_p^2 = .04$. **B. Peak calcium signal magnitude.** Mean magnitude of peak calcium signal differed marginally between conditions, $p = .092$, $\eta_p^2 = .16$. Threat condition: n=10; Compound condition: n=11; Safety condition: n=9. All error bars show +/- 1 SEM. ns = not significant.

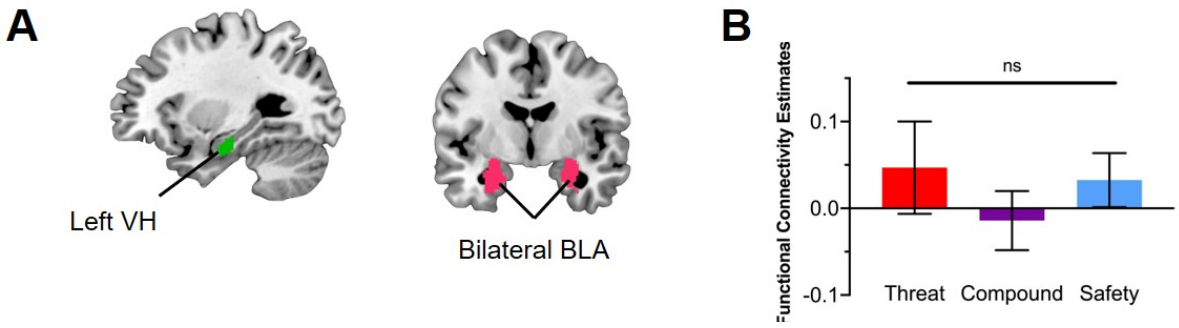

Fig. S10. Ventral hippocampus to basolateral amygdala functional connectivity in humans. A. Regions of interest. The left ventral/anterior hippocampus (VH) region of interest (ROI; green) examined in the present study was obtained from (19). The bilateral basolateral amygdala (BLA) ROI (magenta) was selected from FSL's Juelich histological atlas (22), thresholded at 50% probability, and combined across the two hemispheres. A generalized psychophysiological interaction (gPPI) was implemented in FSL to extract estimates of functional connectivity between these two regions. **B. Functional connectivity results.** No significant effect of condition on functional connectivity was observed, n=48, p = .728, η_p^2 = .01. All error bars show +/- 1 SEM. ns = not significant.

Table S1. Descriptive Statistics of Demographic Variables for Human Participants

Variable	*Mean (SD)*	*Range*
Age, in years	23.42 (3.51)	18 - 30
Sex	22M : 32F	
FSIQ	115.23 (13.37)	84 - 142
Higher Education, n (%)	42 (78%)*	
Race/Ethnicity, n (%)		
Asian	10 (18.5%)	
Black or African American	6 (11.1%)	
Hawaiian/ Pacific Islander	0 (0%)	
Hispanic/Latino	7 (13%)	
Non-Hispanic White/Caucasian	24 (44.4%)	
Other/Unknown	7 (13%)	
Motion-related measures, in mm**		
Absolute motion	0.44 (0.28)	0.08 - 1.38
Relative motion	0.07 (0.03)	0.03 - 0.14
Framewise displacement	0.12 (0.04)	0.07 - 0.19
Outlier timepoints (n)	34.55 (24.23)	0 - 92
Outlier timepoints (%)	3.32% (2.33%)	0 - 8.85%

FSIQ = Full-scale Intelligence Quotient, WASI = Wechsler Abbreviated Scale of Intelligence (7).
***responses missing for 6 participants, **after motion exclusion (n=50)**

Supporting References

1. G. Paxinos, K. B. J. Franklin, *Paxinos and Franklin's The mouse brain in stereotaxic coordinates.*, 4th Ed. (Amsterdam: Academic Press, 2013).
2. M. S. Fanselow, Conditioned and unconditional components of post-shock freezing. *Pavlov. J. Biol. Sci.* **15**, 177–182 (1980).
3. G. Cui, *et al.*, Deep brain optical measurements of cell type–specific neural activity in behaving mice. *Nat. Protoc.* **9**, 1213–1228 (2014).
4. L. A. Gunaydin, *et al.*, Natural Neural Projection Dynamics Underlying Social Behavior. *Cell* **157**, 1535–1551 (2014).
5. J. Akerboom, *et al.*, Optimization of a GCaMP Calcium Indicator for Neural Activity Imaging. *J. Neurosci.* **32**, 13819–13840 (2012).
6. J. D. Power, K. A. Barnes, A. Z. Snyder, B. L. Schlaggar, S. E. Petersen, Spurious but systematic correlations in functional connectivity MRI networks arise from subject motion. *Neuroimage* **59**, 2142–54 (2012).
7. D. Wechsler, *Wechsler Abbreviated Scale of Intelligence* (The Psychological Corporation, 1999).
8. R. C. Oldfield, The assessment and analysis of handedness: the Edinburgh inventory. *Neuropsychologia* **9**, 97–113 (1971).
9. T. A. Brown, D. H. Barlow, *Anxiety and Related Disorders Interview Schedule for DSM-5 (ADIS-5)® - Adult Version* (Oxford University Press, 2014).
10. T. B. Lonsdorf, *et al.*, Don't fear 'fear conditioning': Methodological considerations for the design and analysis of studies on human fear acquisition, extinction, and return of fear. *Neurosci. Biobehav. Rev.* **77**, 247–285 (2017).
11. B. J. Casey, *et al.*, The Adolescent Brain Cognitive Development (ABCD) study: Imaging acquisition across 21 sites. *Dev Cogn Neurosci* (2018) https:/doi.org/10.1016/j.dcn.2018.03.001.
12. M. F. Glasser, *et al.*, The minimal preprocessing pipelines for the Human Connectome Project. *Neuroimage* **80**, 105–24 (2013).
13. J. L. Andersson, S. Skare, J. Ashburner, How to correct susceptibility distortions in spin-echo echo-planar images: application to diffusion tensor imaging. *Neuroimage* **20**, 870–88 (2003).
14. H. Chang, J. M. Fitzpatrick, A technique for accurate magnetic resonance imaging in the presence of field inhomogeneities. *IEEE Trans. Med. Imaging* **11**, 319–329 (1992).
15. P. S. Morgan, R. W. Bowtell, D. J. O. McIntyre, B. S. Worthington, Correction of spatial distortion in EPI due to inhomogeneous static magnetic fields using the reversed gradient method. *J. Magn. Reson. Imaging JMRI* **19**, 499–507 (2004).
16. D. J. Hagler, *et al.*, Image processing and analysis methods for the Adolescent Brain Cognitive Development Study. *bioRxiv* (2018) https:/doi.org/10.1101/457739 (June 14, 2019).
17. M. Jenkinson, P. Bannister, M. Brady, S. Smith, Improved optimization for the robust and accurate linear registration and motion correction of brain images. *Neuroimage* **17**, 825–41 (2002).
18. J. W. Tukey, *Exploratory Data Analysis* (Addison-Wesley Publishing Company, 1977).
19. N. C. Hindy, N. B. Turk-Browne, Action-Based Learning of Multistate Objects in the Medial Temporal Lobe. *Cereb. Cortex N. Y. NY* **26**, 1853–1865 (2016).
20. A. J. Shackman, *et al.*, The Integration of Negative Affect, Pain, and Cognitive Control in the Cingulate Cortex. *Nat. Rev. Neurosci.* **12**, 154–167 (2011).
21. S. Mackey, M. Petrides, Architecture and morphology of the human ventromedial prefrontal cortex. *Eur J Neurosci* **40**, 2777–96 (2014).
22. K. Amunts, *et al.*, Cytoarchitectonic mapping of the human amygdala, hippocampal region

and entorhinal cortex: intersubject variability and probability maps. *Anat Embryol Berl* **210**, 343–52 (2005).
23. D. R. Bach, A head-to-head comparison of SCRalyze and Ledalab, two model-based methods for skin conductance analysis. *Biol. Psychol.* **103**, 63–68 (2014).
24. D. R. Bach, G. Flandin, K. J. Friston, R. J. Dolan, Time-series analysis for rapid event-related skin conductance responses. *J. Neurosci. Methods* **184**, 224–234 (2009).
25. D. R. Bach, K. J. Friston, R. J. Dolan, An improved algorithm for model-based analysis of evoked skin conductance responses. *Biol. Psychol.* **94**, 490–497 (2013).